Endo Hydrogens on Main Group–Transition Metal Clusters. Theoretical Analysis of the Interconversion of FeHFe and EHFe Interactions and Deprotonation of $Fe_3(CO)_9EH_x$ (E = B, x = 5; E = C, x = 4)

Mary M. Lynam, Daniel M. Chipman,[1] Reynaldo D. Barreto, and Thomas P. Fehlner*

Department of Chemistry and Radiation Laboratory, University of Notre Dame, Notre Dame, Indiana 46556

Received April 15, 1987

UV–photoelectron spectroscopy and Fenske–Hall molecular orbital calculations are used to compare the electronic structures of the isoelectronic clusters (μ-H)$_3$Fe$_3$(CO)$_9$(μ_3-CR) (I) and (μ-H)Fe$_3$(CO)$_9$(μ_3-H$_3$BR) (II, R = H, CH$_3$). The orientation of metal-bound carbonyls of structurally characterized trimetal carbonyl clusters with main-group capping atoms is used as an independent indicator of the participation of the metal atom in metal–metal vs metal–main group bonding. These observations, combined with the calculations, allow the perturbation of a capped-trimetal cluster by varying numbers of metal–metal and metal–main group edge bridging hydrogens to be delineated. In turn, these approaches suggest that the distribution of endo hydrogens on a EM$_3$ cluster (E = B, C) depends on a complex, but understandable, interplay among (a) the requirements for good MM vs EM bonding, (b) the perturbation of MM and EM interactions by bridging hydrogens, and (c) a fundamental difference in the EM interaction for E = B vs C. The last factor is shown to reside in the interaction of the pπ orbitals of the ER capping fragment with the trimetal fragment. These results and ab initio main-group cluster model calculations are used to explain the promotion of EHM interactions by the deprotonation of EM$_3$ clusters. Subtle reorganization of the entire cluster structure permits dramatic changes in the structure of the main-group moiety to take place with little change in overall energy.

One of the most prevalent type of transition-metal cluster is the trimetal cluster with a main-group cap (Chart I).[2] Clusters with capping atoms ranging over the central portion of the periodic table and transition metals centered on groups 8 and 9, including examples from all three rows of the periodic table, are known.[2,3] Often, but not always, the principal ligands on the metals are CO or C_5H_5. A topological understanding of metal clusters is summarized in various electron-counting rules.[4] For the capped trinuclear clusters, the electron count is most often 12 (or 48). These conceptual predictors have been supplemented with studies of electronic structure including photoelectron spectroscopic as well as calculational techniques.[5]

Often the main-group and transition-metal fragments supply less than 12 electrons to the cluster bonding and endo-cluster hydrogens make up the difference in the electron count. In a homonuclear capped trimetal system, these hydrogens can bridge either metal–metal edges (faces) or main-group atom–metal edges (faces). Recently we have experimentally demonstrated tautomerism involving metal–metal vs metal–main-group atom bridging hydrogens in the cluster with the composition $Fe_3(CO)_9CH_4$, i.e., tautomers (1,0,3), (1,1,2), and (1,2,1) shown in Chart II where the numbers in parentheses refer to the number of EH(terminal), EHFe, and FeHFe hydrogens, respectively.[6] In addition we have shown that the lowest energy distributions of endo hydrogens on the isoelectronic cluster cores $[Fe_3(CO)_9CH]^{3+}$ and $[Fe_3(CO)_9BH]^{4-}$ are different.[6,7] Indeed, for equal numbers of endo hydrogens, the least stable arrangement of the former corresponds to the most stable arrangement of the latter. Further, the experimental studies demonstrate that deprotonation with the consequent change in overall cluster charge can result in an endo-hydrogen rearrangement.[8] Finally, in work on related tetrametal ferraborane clusters, we have shown that replacement of an exo-cluster CO ligand with a phosphine changes tautomer stabilities in a manner that correlates with the expected perturbation of cluster charge distribution.[9]

Chart I

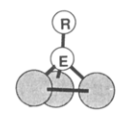

I, E = C
II, E = B

Chart II

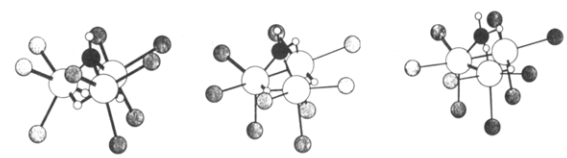

(1,0,3) (1,1,2) (1,2,1)

These results pose some interesting questions concerning the properties of hydrogen atoms on the "surface" of a main group–transition-metal cluster. For example, what is the relationship between E–M and M–M bonding in the EM$_3$ cluster? How does the placement of an endo hy-

(1) Radiation Laboratory.
(2) Johnson, B. F. G., Ed. *Transition Metal Cluster*; Wiley: New York, 1980.
(3) Vahrenkamp, H. *Adv. Organomet. Chem.* **1983**, *22*, 169.
(4) See: Wade, K. *Adv. Inorg. Chem. Radiochem.* **1976**, *18*, 1. Mingos, D. M. P. *Chem. Soc. Rev.* **1986**, *15*, 31 and references therein.
(5) See, for example: Hall, M. B. In *Organometallic Chemistry*; Shapiro, B. L., Ed.; Texas A&M Press: College Station, TX, 1983; p 334. Root, D. R.; Blevins, C. H.; Lichtenberger, D. L.; Sattelberger, A. P.; Walton, R. A. *J. Am. Chem. Soc.* **1986**, *108*, 953. Barreto, R. D.; Fehlner, T. P.; Hsu, L.-Y.; Jan, D.-Y.; Shore, S. G. *Inorg. Chem.* **1986**, *25*, 3572.
(6) Dutta, T. K.; Vites, J. C.; Jacobsen, G. B.; Fehlner, T. P. *Organometallics* **1987**, *6*, 842.
(7) Vites, J. C.; Housecroft, C. E.; Eigenbrot, C.; Buhl, M. L.; Long, G. J.; Fehlner, T. P. *J. Am. Chem. Soc.* **1986**, *108*, 3304.
(8) Vites, J. C.; Jacobsen, G.; Dutta, T. K.; Fehlner, T. P. *J. Am. Chem. Soc.* **1985**, *107*, 5563.
(9) Housecroft, C. E.; Fehlner, T. P. *Organometallics* **1986**, *5*, 1279.

0276-7333/87/2306-2405$01.50/0

drogen on an E–M vs M–M edge affect the other and vice versa? How does deprotonation promote the formation of EHM interactions? Answers to these questions are to be found in the cluster electronic structure. Herein we present information derived from UV–photoelectron spectroscopy and nonparameterized Fenske–Hall calculations that defines the basic electronic structure. In addition, the electronic effects associated with the identity of the capping main-group atom and geometric relationships between exo-cluster ligand placement and hydrogen location are used to provide empirical information on cluster bonding. Finally, the role of deprotonation (or cluster charge) on hydrogen location is explored by using main-group cluster modeling via ab initio calculations. The conclusions are pertinent to the behavior of main-group fragments, including hydrocarbyls, undergoing formal hydrogenation/dehydrogenation on a trimetal atom site as well as to aspects of the general problem of CH bond activation.[10]

Results

Electronic Structure of $Fe_3(CO)_9EH_x$. The essential features of the electronic structure of the capped trimetal cluster system have been effectively presented elsewhere.[5] Here we summarize those components pertinent to the present work as well as present new spectroscopic results on the ferraborane $(\mu\text{-H})Fe_3(CO)_9(\mu_3\text{-}H_3BCH_3)$ ($II(CH_3)$). Our emphasis is on the differences in electronic structures for E = C and B. Although none of the approximate approaches used herein for these complex systems give absolute answers, we do expect them to correctly reflect relative differences between the two isoelectronic systems.

A comparison of the UV photoelectron spectra of $(\mu\text{-H})Fe_3(CO)_9(\mu_3\text{-}H_3BCH_3)$ and $(\mu\text{-H})_3Fe_3(CO)_9(\mu_3\text{-}CCH_3)$ ($I(CH_3)$)[11] (Figure 1) with each other as well as with calculated eigenvalue spectra using the non-parameterized Fenske-Hall technique permits gross differences in electronic structure to be identified. The broader bands of $II(CH_3)$ can be attributed to the lower symmetry. At first sight, there is little to distinguish the two. However, note that although the ionization feature that distinguished $I(CH_3)$ from $Co_3(CO)_9(\mu_3\text{-}CCH_3)$ (band 2)[11] is also present in $II(CH_3)$, it is found at significantly higher ionization potential. This is consistent with the calculations which show that this band is due to FeHFe ionizations in $I(CH_3)$ but is mainly a result of BHFe ionizations in $II(CH_3)$. Second, although the d bands of both compounds show evidence of three components, the splitting in $II(CH_3)$ is less than that in $I(CH_3)$. This is also consistent with the calculations which show that the components of the d band at lower and higher ionization potential contain significant contributions from the capping E atom. With H-bridged MM edges ($I(CH_3)$) the contributions from E are much larger than with H-bridged EM edges ($II(CH_3)$) which is consistent with the magnitude of the splitting observed.

Figure 1 emphasizes the similarity in electronic structure of I vs II. Hence, the factors controlling endo-hydrogen position will be subtle ones and before we can address the question of most stable endo-hydrogen location the differences in cluster cores must be more precisely defined. In order to compare cluster cores in detail, Fenske–Hall calculations were carried out on the anions $[Fe_3(CO)_9EH]^{n-}$

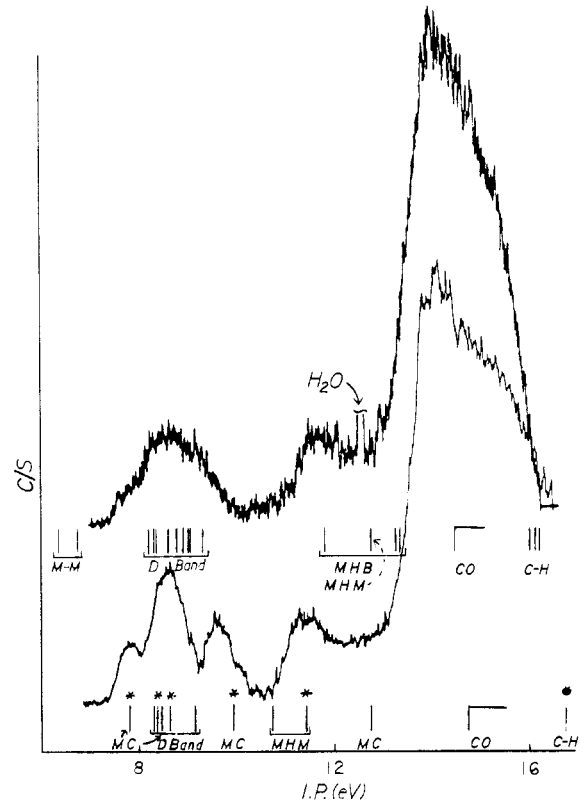

Figure 1. He I photoelectron spectra of $I(CH_3)$, bottom, and $II(CH_3)$, top. The eigenvalue spectra shown are calculated by using the Fenske–Hall technique as indicated in the text. Values shown for the latter are $-0.8[E(MO) + 0.5]$ where $E(MO)$ are the calculated eigenvalues. Degenerate molecular orbitals are indicated with asterisks, and an indication of the MO atomic compositions is given.

(E = B, C; n = 4, 3, respectively). A fragment analysis in terms of $[Fe_3(CO)_9]^{2-}$ and $EH^{(n-2)-}$ resulted in the interaction diagram shown in Figure 2 for E = C. As discussed further below, the results for two limiting relative orientations of the carbonyls are shown. Fully consistent with earlier studies, the E–M_3 bonding results from interactions of the σ and π (relative to the pseudo C_3 axis of the EM_3 cluster) orbitals of the E atom with appropriate orbitals of the M_3 fragment. The diagram for E = B is qualitatively similar and the essential differences in the EH and M_3 interactions for E = B and C are expressed in Figure 3 in terms of the energies of the σ and π orbitals. Note that these energies are derived from the diagonal elements of the Fock matrix in the complete molecule and are not arbitrary.[12] The essential difference between CH^- and BH^{2-} resides in the relative energies of the donor and acceptor orbitals of the $EH^{(n-2)-}$ fragments—a difference that is ultimately due to the lower effective nuclear charge of B vs C. As shown in Figure 3, both the σ and π levels of the BH fragment are at higher energies than those of the CH fragment. The overlap populations shown in the supplementary material show that the differences in energy levels for the CH and BH fragments result in much stronger σ and somewhat weaker π interactions for BH than for CH. We have pointed out previously that in the binding of C_2H_4 and $B_2H_5^-$ to iron, the same trend in strengths of σ and π interactions is found.[13]

The orientation of the carbonyl ligands relative to the cluster framework reflects the electronic structure.[14]

(10) Brookhart, M.; Green, M. L. H. *J. Organomet. Chem.* **1983**, *250*, 395. Crabtree, R. H. *Chem. Rev.* **1985**, *85*, 245.
(11) Wong, K. S.; Fehlner, T. P. *J. Am. Chem. Soc.* **1981**, *103*, 966. Wong, K. S.; Haller, K. J.; Dutta, T. K.; Chipman, D. M.; Fehlner, T. P. *Inorg. Chem.* **1982**, *21*, 3197. DeKock, R. L.; Wong, K. S.; Fehlner, T. P. *Ibid.* **1982**, *21*, 3203.
(12) Kostic, N. M.; Fenske, R. F. *Organometallics* **1982**, *1*, 489.
(13) DeKock, R. L.; Deshmukh, P.; Fehlner, T. P.; Housecroft, C. E.; Plotkin, J. S.; Shore, S. G. *J. Am. Chem. Soc.* **1983**, *105*, 815.

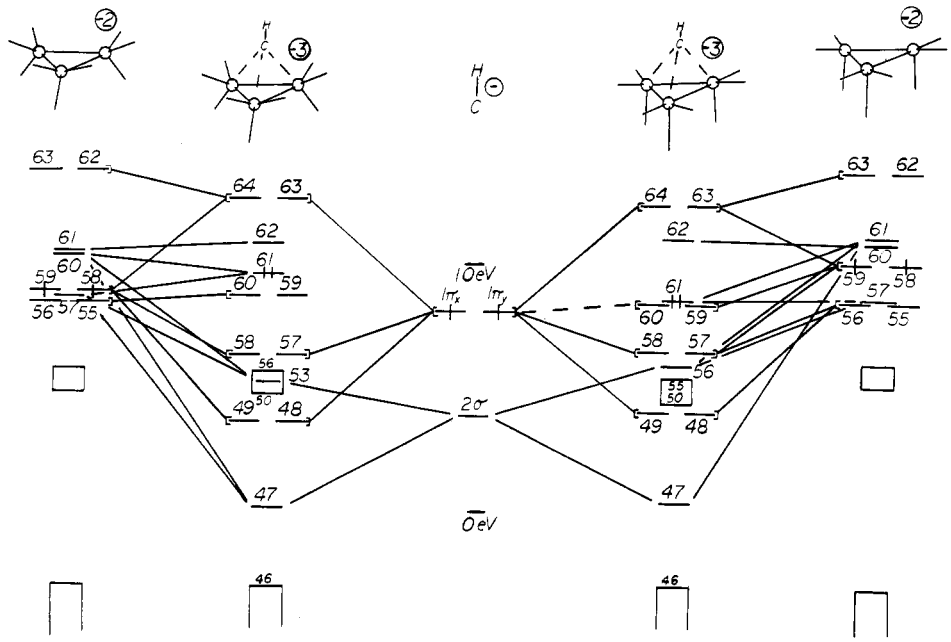

Figure 2. Correlation diagram for $[Fe_3(CO)_9CH]^{3-}$ as formed from CH- and either $[Fe_3(CO)_9]^{2-}$ "tilted" (left-hand side) or $[Fe_3(CO)_9]^{2-}$ "flat" (right-hand side). Correlation lines are drawn on the basis of a fragment analysis of the Fenske-Hall calculations.

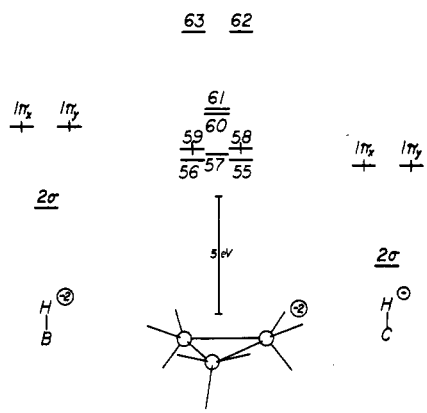

Figure 3. Comparison of the energies of the frontier orbitals of BH^{2-} and CH^- relative to those of $[Fe_3(CO)_9]^{2-}$. The orbitals are all on the same energy scale with the positions of the main-group fragment orbitals being given relative to those of the metal fragment. All energies are taken from the Fock matrix for the complete molecule and are not arbitrary.

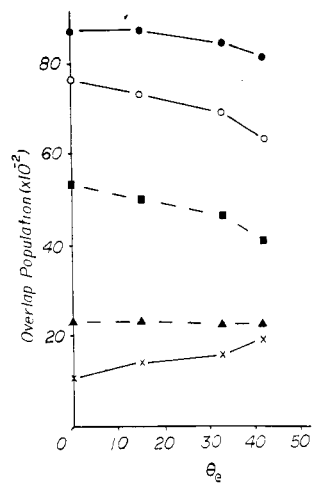

Figure 4. Plot of selected overlap populations as a function of the "tilt" angle (θ_e) (Chart I) for $[Fe_3(CO)_9CH]^{3-}$: closed cirles, total overlap; open circles, total Fe_3–C overlap; closed squares and triangles, π-Fe_3–C and σ-Fe_3–C, respectively; ×, Fe_3 overlap.

Hence, the observed orientation of the carbonyl ligands can serve as a reporter of the cluster bonding insofar as the metals are concerned. In the following we define this relationship for EM_3 clusters and then examine the effect of bridging ligands. Structures with "tilt" angles, θ as defined in Chart III, varying between 0° and 42° have been explored with the Fenske–Hall technique. Changing the orientation of the CO's does not change the qualitative nature of the HE–Fe_3 interaction as exemplified for I in Figure 2; however, the strengths of the interactions do change. The relative strengths of the E–M and M–M interactions as a function of "tilt" angle are revealed by the Mulliken overlap populations. These are plotted in Figure 4 for E = C and show that the M–M interactions are favored by greater "tilt" while E–M interactions are favored by less "tilt". The former is true for the M_3 fragment along as well. Clearly, the requirements for good M–M bonding are opposed to those for good E–M bonding.[15] As described above, the HE–M_3 fragment–fragment

Chart III

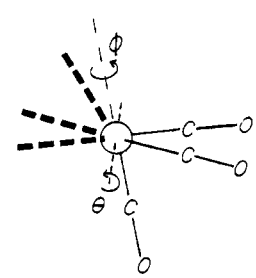

overlap consists of σ and π components. Although the σ component remains nearly constant with increasing "tilt" angle, the π component decreases substantially. The same qualitative trend holds for E = B and, hence, a key in-

(14) Hoffmann, R.; Schilling, B. E. R.; Bau, R.; Kaesz, H. D.; Mingos, D. M. P. *J. Am. Chem. Soc.* **1978**, *100*, 6088.

(15) The magnitude of the changes in the E–M overlaps relative to those of the M–M overlaps might suggest a more important role for the former; however, caution must be exercised when overlaps are compared between very different atom types. On the other hand, it is known that bridging and capping ligands stabilize metal clusters with respect to degradation.[3]

teraction is the decrease at larger "tilt" angles of the overlap of the capping atom π functions with the M_3 framework orbitals. This is reasonable as at low "tilt" angles the π acceptor orbitals of the metal fragment are pointed more directly at the points of maximum amplitude of the $p\pi$ orbitals of the main-group capping atom. Although both boron and carbon show the same qualitative effects, the σ interaction constitutes a higher percentage of the total for boron (41 vs 34%) and the π interaction for boron is more sensitive to "tilting" than that for carbon (There is a 40% change in going from 0° to 42° for boron vs a 23% change for carbon). Simply put, the larger boron 2s orbital overlaps more effectively with the metal orbitals and the larger boron 2p requires a low "tilt" angle for effective π overlap. All this suggests that in any real example an observed "tilt" angle will express the balance between the requirements of the capping atom for good π overlap and the requirements of the metals for good M–M overlap. This is corroborated in the structural data presented below. As shown below, the differences between B anc C as capping atoms as revealed by these calculations partially determine which edges are most effectively bridged.

Carbonyl Orientation as a Probe of Bonding. If the calculated trends presented immediately above are correct, then variation in the nature of E should result in predictable variation in the observed orientations of the carbonyls on structurally characterized EM_3 clusters. A significant number of structures have been reported and the pertinent information is given in Table I. The CO "tilt" (θ) and "twist" (ϕ) angles were calculated from published crystallographic data. The data on systems with first-row transition metals are used to parameterize eq 1

$$\theta_e = 17.8 + A \quad (1)$$

for various E atoms. The constant of 17.8 is a "tilt" angle derived from an idealized $M_4(CO)_{12}$ cluster with six MM bonds of equal length and (OC–M–CO) angles of 90°.[16] Ignoring CO–CO repulsion, this angle will be independent of MM bond distance. θ_e is the angle between the plane defined by the metal triangle and the equatorial CO's. θ_a, also given in Table I, is the angle between the metal triangle and the axial CO and provides similar information. The value A represents the change in "tilt" angle that results from the replacement of the capping $M(CO)_3$ fragment with the main-group atom E. A good fit (the deviations of observed and calculated values are given in Table I) for first-row capping atoms yields $A = 12.0$ while for second- and third-row capping atoms $A = 6.5$. That is, in agreement with the calculations above, the smaller the capping atom, the greater the "tilt" angle; e.g., for the same metal SR has a smaller "tilt" angle than CR. The parameter A, then, gives us an empirical measure of the balance between the E–M and M–M interactions. For comparative purposes in the discussion below, the effect of "tilt" on the metal octahedral bond vectors pointing toward the capping E atom is shown in Figure 5 for the ideal θ_e of 17.8; the observed θ_e for $Co_3(CO)_9CR$ and a θ_e of 0. Note that Schmid[17] previously suggested that the size of E relative to the metals apparently places limitations on the existence of EM_3 clusters.

Obviously, the placement of bridging hydrogens on E–M or M–M edges will change the net main group–metal or

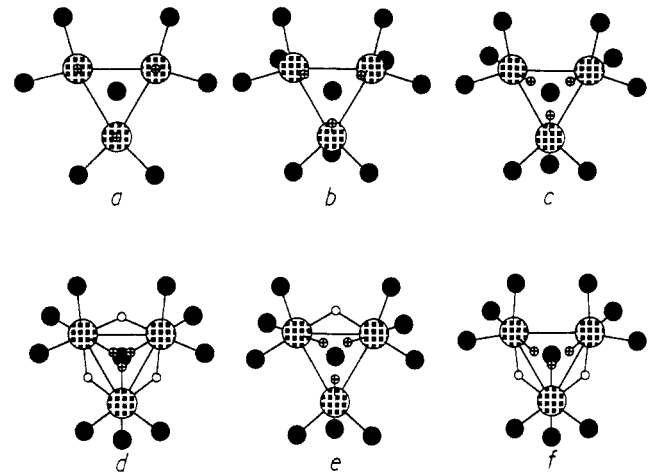

Figure 5. Schematic representation of the orientation of the octahedral bond vectors from the $Fe(CO)_3$ fragments relative to the capping E atom. The perspective is looking down the pseudo C_3 axis from above the E atom. The small circles with plus signs represent the point of intersection of the octahedral bond vector of Fe trans to the axial CO with a plane containing E and lying parallel to the M_3 plane: (a) 0° "tilt", (b) 17.8° "tilt", (c) 29.5° "tilt", (d) 43° "tilt" for three MHM, (e) ideal "tilt" and "twist" for one MHM, (f) ideal "tilt" and "twist" for two MHM.

metal–metal edge interactions. The steric and electronic effect of endo hydrogens (hydrides) in metal clusters is a well-established fact,[18] and the presence of M–M bridging hydrogens, even when not directly located crystallographically, is often revealed by the spatial arrangement of other ligands and the metal atoms. The effects of M–H–M hydrogens is most easily seen in a comparison of isoelectronic molecules. For example, in earlier work we have pointed out a correlation between the orientation of the exo-carbonyl ligands relative to the metal plane in $H_3Fe_3(CO)_9CCH_3$ and $Co_3(CO)_9CCH_3$ and the apparent metal octahedral bond vectors.[11] The presence of three MHM hydrogens induces an increase in the average "tilt" of the axial and equatorial carbonyls of 14°. The generality of this point as well as the dependence on metal atom can be tested with the data in Table I. For systems with three MHM bridging hydrogens eq 2 expresses the "tilt" angle

$$\theta_e = 30.6 + A + B \quad (2)$$

and the deviations between calculated and observed values of θ_e are given in Table I. A is the same as in eq 1 while B is 0.0, 1.3, and 3.9 for first-, second-, and third-row metals, respectively. This parameterization of the structural data allows two conclusions to be drawn. First, in accord with the calculations, increasing the MM distance with a fixed capping atom increases the "tilt" angle. Note that the "tilt" angle of the only system with a non-first-row metal and no bridging hydrogens, $Ir_3(CO)_9Bi$, is fit well by adding B to eq 1. Again this is consistent with a model in which E–M π interactions are important. Second, the bridging hydrogens induce an additional "tilt" of 12.8° independently of metal and capping atom identities. This is expressed by the increase in the constant in eq 1 from 17.8 to 30.6. Thus, the previously reported observation for the single Fe_3 system is valid in general. The observed CO orientations show that the bonding requirements of MHM edges of the EM_3 cluster take precedence over those of unbridged edges in that the balance in the competition

(16) The use of a more realistic, but less convenient, C–M–C angle of 100° would reduce the value of the constant but does not change the conclusions based on the equation. The "tilt" angles in the structure of $Ir_4(CO)_{12}$ lie between 8 and 15°: Churchill, M. R.; Hutchinson, J. P. *Inorg. Chem.* **1978**, *12*, 3528.

(17) Schmid, G. *Angew. Chem., Int. Ed. Engl.* **1978**, *17*, 392.

(18) Teller, R. G.; Bau, R. *Struct. Bonding (Berlin)* **1981**, *44*, 1. Bau, R., Ed. *Transition Metal Hydrides*; Advances in Chemistry 167; American Chemical Society: Washington, D.C., 1978.

Table I. "Tilt" and "Twist" Angles (deg) for $H_nM_3(CO)_9X$ Clusters (n = 0–3)

compd[y]	M_1	M_2	M_3	Δ_0[z]	ref
$Co_3(CO)_9CH$					
θ_e	31.1 (1)	31.5 (1)	32.4 (1)	−1.9	*a*
θ_a	101.1	101.0	102.7		
ϕ	0.9	−0.1	1.4		
$Co_3(CO)_9CMe$					
θ_e	30.0 (7)	29.1 (3)	29.0 (2)	0.4	*b*
θ_a	101.4	101.3	99.4		
ϕ	1.1	1.8	1.4		
$Co_3(CO)_9CCl$					
θ_e	31.2 (3)	28.8 (4)	31.8 (5)	−0.8	*c*
θ_a	100.5	101.0	101.2		
ϕ	1.1	1.9	0.6		
$Co_3(CO)_9S$					
θ_e	26.7 (29)	24.6 (17)	24.9 (22)	−1.1	*d*
θ_a	97.3	98.9	96.8		
ϕ	1.0	1.7	0.3		
$Co_3(CO)_9Se$					
θ_e	22.5 (9)	23.2 (6)	24.3 (7)	−1.0	*e*
θ_a	96.7	97.4	98.4		
ϕ	1.3	0.4	1.9		
$FeCo_2(CO)_9Se$					
θ_e	21.3 (5)	22.8 (3)	24.0 (5)	1.6	*e*
θ_a	96.6	98.5	97.9		
ϕ	0.3	0.8	2.1		
$FeCo_2(CO)_9Te$					
θ_e	22.5 (4)	21.8 (3)	20.6 (5)	2.7	*e*
θ_a	96.9	97.9	95.6		
ϕ	1.6	0.6	1.2		
$FeCo_2(CO)_9S$					
θ_e	25.0 (16)	23.5 (11)	24.5 (12)	0.0	*f*
θ_a	95.7	100.7	98.6		
ϕ	−0.1	0.8	0.5		
$FeCo_2(CO)_9NH$					
θ_e	28.0 (2)	27.1 (1)	27.1 (1)	2.4	*g*
θ_a	100.5	103.6	101.2		
ϕ	0.0	1.5	0.0		
$Fe_3(CO)_9S(C_4H_9)^-$					
θ_e	20.6 (5)	21.0 (5)	21.6 (5)	3.2	*h*
θ_a	95.6	96.0	95.5		
ϕ	−0.3	1.4	1.9		
$Ir_3(CO)_9Bi^*$					
θ_e	28.4 (17)	30.2 (11)	26.7 (18)	−0.2	*i*
θ_a	98.7	95.5	95.7		
ϕ	0.7	1.5	1.0		

	M_2	M_1H	M_3H	Δ_0[z]	Δ_1[z]	ref
$HFe_3(CO)_9H_3BH$						
θ_e	13.9 (8)	17.8 (8)	16.2 (8)			*j*
θ_a	97.0	100.1	98.2			
ϕ	1.6	8.9	7.7			
$HFe_3(CO)_9S(C_3H_7)$						
θ_e	21.5 (8)	23.6 (8)	25.2 (9)	2.8	6.3	*k*
θ_a	98.0	101.4	101.1			
ϕ	0.4	5.9	3.0			
$HFe_3(CO)_9S(C_6H_{11})$						
θ_e	23.0 (11)	23.4 (8)	23.6 (10)	1.3	7.2	*l*
θ_a	99.2	100.7	99.7			
ϕ	0.4	3.0	2.3			

	M_1H	M_3H	$M_2(H)_2$	Δ_1[z]	Δ_2[z]	ref
$H_2Fe_3(CO)_9PPh$						
θ_e	28.8 (3)	32.1 (3)	38.0 (4)	0.3	−0.9	*l*
θ_a	102.0	106.1	114.5			
ϕ	5.2	3.2	0.8			
$H_2Ru_3(CO)_9NPh$						
θ_e	29.7 (3)	31.9 (3)	39.0 (2)	6.7	4.9	*m*
θ_a	111.6	113.0	124.5			
ϕ	3.2	2.5	0.9			
$H_2Ru_3(CO)_9PPh$						
θ_e	31.6 (8)	27.6 (8)	40.9 (8)	2.4	−2.5	*n*
θ_a	104.9	103.9	118.3			
ϕ	3.7	3.7	0.3			
$H_2Ru_3(CO)_9S$						
θ_e	26.7 (3)	29.9 (4)	36.8 (2)	3.7	1.6	*o*
θ_a	106.0	110.2	118.7			
ϕ	5.0	3.3	1.9			
$H_2Os_3(CO)_9CCO$						
θ_e	29.7 (5)	29.7 (5)	36.8 (9)	16.4	9.7	*p*
θ_a	110.2	110.2	121.9			
ϕ	2.6	2.6	0.0			
$H_2Os_3(CO)_9NMe$						
θ_e	35.8 (3)	35.8 (3)	48.3 (3)	4.3	−1.8	*q*
θ_a	119.6	119.6	126.9			
ϕ	1.3	1.3	0.0			
$H_2Os_3(CO)_9S$						
θ_e	27.1 (1)	27.3 (1)	36.0 (2)	7.4	5.0	*r*
θ_a	106.6	106.0	122.0			
ϕ	2.4	5.3	1.2			

	$M_1(H)_2$	$M_2(H)_2$	$M_3(H)_2$	Δ_3[z]	ref
$H_3Fe(CO)_9CMe$					
θ_e	41.6 (5)	41.4 (5)	44.0 (5)	0.3	*s*
θ_a	119.9	119.1	121.8		
ϕ	1.1	0.1	0.5		
$H_3Fe_3(CO)_9Bi$					
θ_e	38.6 (3)	37.6 (4)	36.1 (4)	−0.3	*t*
θ_a	117.0	115.0	114.2		
ϕ	0.5	−0.2	0.0		
$H_3Ru_3(CO)_9CMe$					
θ_e	43.8 (4)	43.5 (4)	43.8 (4)	0.2	*u*
θ_a	124.2	124.6	124.2		
ϕ	0.2	0.0	0.2		
$H_3Ru_3(CO)_9CCl$					
θ_e	44.0 (1)	44.4 (1)	44.0 (1)	−0.2	*v*
θ_a	123.4	123.7	123.4		
ϕ	2.8	0.0	−2.8		
$H_3Os_3(CO)_9CH$					
θ_e	45.8 (0.3)	45.4 (0.4)	45.8 (0.4)	0.8	*w*
θ_a	125.8	126.2	128.2		
ϕ	0.4	1.6	1.1		
$H_3Os_3(CO)_9BCO$					
θ_e	49.3 (7)	43.5 (6)	49.0 (4)	−0.8	*x*
θ_a	120.8	124.6	120.9		
ϕ	0.0	1.0	2.0		

[a] Leung, P.; Coppens, P.; McMullan, R. K.; Koetzle, T. F. *Acta Crystallogr., Sect. B: Struct. Crystallogr. Cryst. Chem.* **1981**, *B37*, 1347. [b] Sutton, P. W.; Dahl, L. F. *J. Am. Chem. Soc.* **1967**, *89*, 261. [c] Bartl, K.; Boese, R.; Schmid, G. *J. Organomet. Chem.* **1981**, *206*, 331. [d] Wei, C. H.; Dahl, L. F. *Inorg. Chem.* **1967**, *6*, 1229. [e] Strouse, C. E.; Dahl, L. F. *J. Am. Chem. Soc.* **1971**, *93*, 6032. [f] Stevenson, D. L.; Wei, C. H.; Dahl, L. F. *J. Am. Chem. Soc.* **1971**, *93*, 6027. [g] Fjare, D. E.; Keyes, D. G.; Gladfelter, W. L. *J. Organomet. Chem.* **1983**, *250*, 383. [h] Winter, A.; Zsolnai, L.; Huttner, G. *Chem. Ber.* **1982**, *115*, 1286. [i] Kruppa, W.; Blaser, D.; Boese, R.; Schmid, G. *Z. Naturforsch., B: Anorg. Chem., Org. Chem.* **1982**, *37B*, 209. [j] Vites, J.; Housecroft, C. E.; Eigenbrot, C.; Buhl, M. L.; Long, G. L.; Fehlner, T. P. *J. Am. Chem. Soc.* **1986**, *108*, 3304. [k] Bau, R.; Don, B.; Grentrey, R.; Haines, R. J.; Love, R. A.; Wilson, R. D. *Inorg. Chem.* **1975**, *14*, 3021. [l] Huttner, G.; Schneider, J.; Mohr, G.; Von Seyerl, J. *J. Organomet. Chem.* **1980**, *191*, 161. [m] Bhaduri, S.; Gopalkrishnan, K. S.; Clegg, W.; Jones, P. G.; Sheldrick, G. M.; Stalke, D. *J. Chem. Soc., Dalton Trans.* **1984**, 1765. [n] Iwaski, F.; Mays, M. J.; Raithby, P. R.; Taylor, P. L.; Wheatley, P. J. *J. Organomet. Chem.* **1981**, *213*, 185. [o] Adams, R. D.; Katahira, D. A. *Organometallics* **1982**, *1*, 53. [p] Shapley, J. R.; Strickland, D. S.; St. George, G. M.; Churchill, M. R.; Bueno, C. *Organometallics* **1983**, *2*, 185. [q] Lin, Y. C.; Knobler, C. B.; Kaesz, H. D. *J. Organomet. Chem.* **1981**, *213*, C41. Lin, Y. C. Ph.D. Thesis, UCLA, 1981. [r] Johnson, B. F. G.; Lewis, J.; Pippard, D.; Raithby, P.; Sheldrick, G. M.; Rouse, K. D. *J. Chem. Soc., Dalton Trans.* **1979**, 616. [s] Wong, K. S.; Haller, K. J.; Dutta, T. K.; Chipman, D. M.; Fehlner, T. P. *Inorg. Chem.* **1982**, *21*, 3197. [t] Whitmire, K. H.; Lagrone, C. B.; Rheingold, A. L. *Inorg. Chem.* **1986**, *25*, 1229. [u] Sheldrick, G. M.; Yesinowski, J. P. *J. Chem. Soc. Dalton Trans.* **1975**, 873. [v] Zhu, N. J.; Lecomte, C.; Coppens, P.; Keister, J. B. *Acta Crystallogr., Sect. B: Struct. Crystallogr. Cryst. Chem.* **1982**, *B38*, 1286. [w] Orpen, A. G.; Koetzle, T. F. *Acta Crystallogr., Sect. B: Struct. Crystallogr. Cryst. Chem.* **1984**, *B40*, 606. [x] Shore, S. G.; Jan, D.-Y. Hsu, L.-Y. Hsu, W.-L. *J. Am. Chem. Soc.* **1983**, *105*, 5923. [y] θ_e refers to equatorial CO's and θ_a to axial CO's. [z] Deviation of calculated (eq 1 or 2) from observed angle θ_e. Δ_0, Δ_1, and Δ_2 refers to metals with 0, 1, and 2 MHM interactions.

for the metal cluster orbitals shifts away from the main group–metal interactions. This shows up dramatically in Figure 5d where one can see that the octahedral bond vectors pointing toward the E atom are very poorly oriented for interaction with the π orbitals of the E atom.[19]

The clusters with one and two bridging hydrogens are more complex in that the $M(CO)_3$ fragments both "tilt" and "twist" (Chart III). As the $H_3M_3(CO)_9E$ systems exhibit a 12.8° "tilt" for two MHM bridges, one can assign a 6.4° "tilt" per MHM bridge. Note now that the $HFe_3(CO)_9(H_3BH)$ cluster exhibits a nearly "flat" $M_3(CO)_9$ fragment and the two bridged $M(CO)_3$ groups are each rotated 8.3° away from the MHM bridge. This is taken to be the "twist" introduced by a MHM bridge. Note that when a metal atom is doubly bridged the "twists" cancel, being equal and in opposite directions. The observed "tilts" and "twists" for the mono- and dibridged clusters are given in Table I. Note that the "tilts" observed are less than those predicted from eq 2 and that the largest deviations are for metals coordinated to one MHM. This suggests the existence of some factor that prevents the metal fragment from adopting the expected "tilt" angle. From the discussion above we suggest that this factor is associated with the requirements for strong EM_3 bonding which is favored by low "tilt" angles. Likewise all the calculated "twist" values are about double those observed. This suggests in the systems without EHM bridges there are interactions that restrict "twisting" of the $M(CO)_3$ fragments.

The idealized structures in Figure 5e,f allow the electronic factors restricting the "twisting" of the $M(CO)_3$ groups to be demonstrated. These diagrams for the EM_3H and EM_3H_2 clusters allow comparison with the EM_3 and EM_3H_3 systems. One can see in Figure 5e that, relative to the unbridged system (Figure 5b), the addition of a single MHM hydrogen orients the bridged metal bond vectors toward the E atom. This suggests that the E pπ interaction parallel to the MHM edge should be less than the perpendicular one. Indeed the overlap of the E pπ orbital perpendicular to the bridged edge is unchanged from that in the M_3E system while that parallel is reduced 11%. For two MHM hydrogens (Figure 5f) there is further rotation of the metal bond vectors particularly for the metal bonded to two hydrogens. The E pπ interaction is again unsymmetrical, and the calculated π-E–M overlaps show the differences predicted by the diagram. That is, the overlap parallel to the unbridged edge is 5% less and that perpendicular is 16% less than in the M_3E system. The net EM π-overlap populations for the EM_3H_x (x = 0–3) are 0.463, 0.438, 0.415, and 0.409, respectively. Note that the differences between the systems with x = 0, 1, and 2 are uniform while that between x = 2 and 3 is much smaller. Hence, as far as the E pπ overlaps are concerned, M_3H_2 and M_3H_3 are equally bad arrangements, and when the M_3H_3 system is deprotonated, a significant increase in stability is achieved if rearrangement to the M_3H system takes place.

There is only one structurally characterized EM_3 cluster with EHM interactions (II), and it also contains a MHM interaction to confuse the issue. However, as shown above, a single MHM interaction has virtually no effect on the exo-CO ligand orientation of the metal with no bridging hydrogens. In order to fit the observed "tilt" angle at the unbridged metal of II with eq 2, the numerical constant required is 13.9 rather than 30.6. In other words, while the carbonyls of a metal center with two MHM bridges undergo an increase of 12.8° in "tilt" angle, the presence of an EHM bridge reduces the "tilt" by 16.7° relative to the unbridged system. This large reduction shows that the requirements of the bridged E–M edge now take precedence over the M–M requirements. Further, the low "tilt" angles of the CO's at the other two irons of II suggest that the requirements of the two EHM bridges also outweigh those of the MHM bridge.

Tautomer Preferences. These observations enable us to postulate an answer to the question of relative stabilities of the four possible tautomers of $[Fe_3(CO)_9EH_4]^{n-}$: (1,0,3), (1,1,2), (1,2,1), and 1,3,0) (see Chart II). For E = B, n = 1, tautomer (1,2,1) is the most stable whereas for E = C, n = 0, the stability order is (1,0,3) > (1,1,2) > (1,2,1). Although (1,3,0) cannot be eliminated as a possible structure, it is not a likely possibility. Indeed for E = C, the HCH angle for reasonable CH and HM distances in the CHM interaction is too acute for (1,3,0) to be an acceptable structure. Even in II where the longer BH and shorter HM distances in the BHM interaction are more accommodating, the calculated HBH angle is 94°. Therefore only structures (1,0,3), (1,1,2), and (1,2,1) are considered in the following discussion.[20] The key point is the inversion in stability going from E = B^- to C. As substantiated in the previous section, the requirements of the MM and EM edges, bridged or unbridged, are competitive. Hence, as M = Fe in both cases, the difference in stability orders results from a perturbation of the balance between these competing interactions by the different main-group atoms. For E = C, the observed stability order shows that a reasonable $CM_3\pi$ interaction obtains even at the large "tilt" angle required for the three MHM interactions. That is, satisfying the requirements of three MHM interactions in (1,0,3) results in a greater stabilization than one CHM plus two MHM (1,1,2) or CHM plus one MHM (1,2,1). On the other hand, with boron, the π overlap, though a smaller proportion of the total EM_3 interaction, decreases drastically with increasing "tilt" angle. The structural analyses given above show that the requirement for an effective π EM interaction is an important component of the cluster total energy, and thus, changing from C to B destabilizes (1,0,3) relative to (1,2,1). Keep in mind that the energy differences between tautomers are on the order of 1 kcal/mol.[6]

We have shown that the deprotonation of II results in a rearrangement in the endo hydrogens to produce as the principal tautomer $[(\mu\text{-H})Fe_3(CO)_9HCH]^-$ rather than $[(\mu\text{-H})_2Fe_3(CO)_9CH]^-$. As the capping atom has not changed, the factors favoring the observed endo-hydrogen rearrangement are even more subtle. As demonstrated above, the requirements for strong MM interactions are competitive with those for strong EM interactions. Likewise, the requirements of bridged interactions take precedence over unbridged. The one known factor that counters the balance favoring (1,0,3) over (1,1,2) in the neutral system is the significant gain in net EM_3 overlap in going from the M_3H_2 to M_3H arrangements. Because of the availability of a number of structures with differing most stable endo-hydrogen locations of similar energies, the simple loss of a MHM proton on deprotonation constitutes a large relative perturbation of the system. In terms of the main-group fragment then, small perturbations in an absolute sense can cause the "reduction/oxidation" of the EH moiety.

(19) These arguments are presented totally in terms of electronic effects. Clearly, there is a steric component, but there is insufficient information to make the distinction.

(20) A structure with no EH terminal hydrogen is also not considered as the calculations indicate that this tautomer is much less stable than those shown.

Chart IV

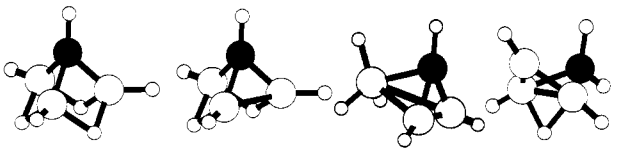

IIIa IIIb IIIc IIId

Table II. Relative Energies (kcal/mol) as a Function of Basis Set and Application of Configuration Interaction

basis	IIIb[a]	IIIc[b]	IIId[b]
STO-3G	37.5	(0.0)[c]	19.3
6-31G	26.4	(0.0)[c]	11.7
CID/6-31G[d]	23.8	(0.0)[c]	13.6

[a] Hypothetical structure—see text. [b] Structures optimized at STO-3G level. [c] Total energies (au): −113.8340, −115.2572, and −115.5680, respectively. [d] Configuration interaction with inclusion of all double excitations.

Main-Group Models for Deprotonation. Previously, we have profitably discussed the geometric and electronic structure of $H_3Fe_3(CO)_9CCH_3$ using the hypothetical isolobal main-group cluster model $H_3(BH)_3CCH_3$ structurally characterized with ab initio techniques.[11] Hence, the same approach is now applied to the problem posed by deprotonation[21] of $Fe_3(CO)_9EH_x$ using $H_3(BH)_3CH$ (IIIa), as a model.

A BHB proton was removed from the fully optimized structure of IIIa to generate a reasonable starting point (IIIb) for the optimization of the anion. Much to our surprise, all attempts to optimize a structure like IIIb failed; the cage opened, and a "classical" structure IIIc resulted. Since there is some question as to whether minimal and split-valence basis sets are adequate for description of a structure such as IIIb, two further calculations were carried out with an augmented 3-21G basis. In the first, diffuse functions were added to all atoms to allow for expansion of the charge distribution of the anion relative to that of the neutral. In the second, polarization functions were added to all heavy atoms and to the bridging hydrogens to better allow for the large strain energies involved in the closed-cage structure. In both cases, geometry optimization still led to the "classical" structure IIIc, giving more confidence in the conclusion that IIIb is not a local minimum structure. The energy of the fully optimized geometry of the latter is compared to that for a point calculation on IIIb in Table II. Clearly, deprotonation is not a small perturbation in this cluster system; i.e., loss of a proton induces considerable structural change.[22]

In the absence of corrections for electron correlation, calculations are prejudiced toward a "classical" vs "nonclassical". Hence, energies of structures IIIb–d were obtained with expanded basis sets plus configuration interaction. The results (Table II) show that although the "nonclassical" structures are stabilized relative to the "classical", no reversal in stabilities is seen. Keep in mind that IIIb is a hypothetical structure and IIIc and IIId have minimum basis set geometries.

As the "classical" structure is not relevant to the transition-metal problem, starting points other than IIIb were explored. Beginning with two of the hydrogens of $CB_3H_6^-$ interacting with carbon, the "butterfly" structure IIId was fully optimized. The energy of this structure (Table II) is intermediate between that of IIIb and IIIc, and the structure itself is strikingly similar to that of $[(\mu\text{-H})Fe_3(CO)_9HCH]^-$.[6] The main difference between them is that the large dihedral angle of the IIId "butterfly" prevents one of the CH bonds from interacting with the tricoordinate boron. This probably reflects the preference of the "hinge" borons for a tetrahedral geometry; i.e., formation of a CHB interaction is not sufficiently exothermic to compensate for a more strained geometry. The fact that the main-group model IIId is stable in the open form while the iron system can be opened as in Figure 6 without massive disruption of the bonding system (see below) suggests that displacement of the CH bond pair from the metal center by a Lewis base may readily occur by attack at the metal. Finally, the production of CH_4 from I, the production of CH_3R from the ruthenium and osmium analogues of I,[23,24] and the production of BH_3 base adducts from $[HFe_3(CO)_9(H_2BH)]^-$[25] may well occur by a mechanism including base displacement of an E–H bond pair from the transition metal.

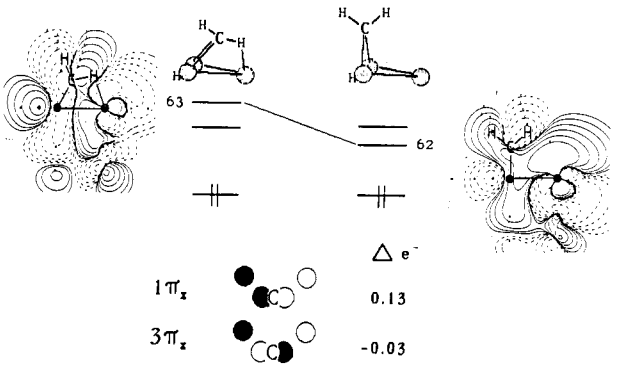

Figure 6. Selected results of calculations on the $[HFe_3(CO)_9(HCH)]^-$ cluster showing effects of breaking the CHFe interaction. These are the reduction in the HOMO–LUMO gap, the creation of an empty orbital on the unique iron (contour diagram of MO 62 at the right), and the change in population of important bonding and antibonding orbitals.

Making and Breaking of a CHFe Interaction in a Cluster. To further relate these model calculations to the transition-metal system, a fragment analysis was carried out on $[(\mu\text{-H})Fe_3(CO)_9(\mu_3\text{-HCH})]^-$. The most informative results are abstracted in Figure 6. Keeping the HCH angle and CH distances constant, the CH_2 fragment is rotated around the H-bridged FeFe axis, thereby moving it away from the unique Fe as shown in the right-hand stick diagram, to generate the metal analogue of IIId. In doing so, a high-lying empty orbital (63) is substantially stabilized, reducing the highest occupied molecular orbital (HOMO)–lowest unoccupied molecular orbital (LUMO) gap. As shown by the orbital contour diagram for MO 62 at the right of Figure 6, this empty orbital is centered on the unique Fe. In rotating the CH_2 fragment away from the unique Fe, a CH bonding orbital ($1\pi_x$) is populated while a CH antibonding orbital ($3\pi_x$) is depopulated. The former effect is significantly larger than the latter.[26]

(21) Lynam, M. M. M.S. Thesis, University of Notre Dame, 1985.

(22) Protonation in other cluster systems is equally effective in inducing structural change. Brint, P.; Healy, E. F.; Spalding, T. R.; Whelan, J. *Chem. Soc., Dalton Trans.* **1981**, 2515. Evans, J. *Ibid.* **1978**, *25*. Cavanaugh, M. A.; Fehlner, T. P.; Stramel, R.; O'Neill, M. E.; Wade, K. *Polyhedron* **1985**, *4*, 687.

(23) Duggan, T. P.; Barnett, D. J.; Muscatella, M. J.; Keister, J. B. *Abstr. Pap.-Am. Chem. Soc.* **1984**, *188th*, INORG 251.

(24) Calvert, R. B. Ph.D. Thesis, Univ. Illinois, Urbana, 1978. As referenced by: Muetterties, E. L. *Chem. Soc. Rev.* **1982**, *11*, 283.

(25) Housecroft, C. E.; Fehlner, T. P. *J. Am. Chem. Soc.* **1986**, *108*, 4867.

There are some significant differences between the cluster system illustrated by $[(\mu\text{-H})Fe_3(CO)_9HCH]^-$ and a typical mononuclear complex containing a CHFe interaction.[10,26] The most obvious difference is that the unsaturated site with which the CH bond pair interacts is on a metal atom other than the one(s) to which the carbon is directly bonded. Second, in contrast with mononuclear systems where σ donation of a CH bond to an unsaturated metal atom is suggested as the driving force for CH bond weakening, here depopulation of the σ level is accompanied by significant population of the σ^* level. As the latter is the suggested mode of activation for metal surfaces,[26] the activation of the CH bond in this trimetal system does indeed lie between that in a mononuclear complex and that in a fragment bound to an extended metal surface. Third, the CH bond forming the CHFe interaction on $[(\mu\text{-H})Fe_3(CO)_9HCH]^-$ does not satisfy any simple electron deficiency of the unique iron atom. In fact, after the CH_2 unit is bent away from the unique iron atom, the electronic charge on this metal atom is increased by about 0.1.

Conclusions

The lowest energy placement of endo hydrogens on a trimetal main-group capped cluster is seen to be the end result of several competing factors. One important factor is the variation in the main group–metal triangle π interaction with the nature of the capping atom. Reducing the effective nuclear charge of the capping atom by going from C to B or by increasing the overall negative charge on the cluster results in a stabilization of EHM interactions relative to MHM interactions. Second, both the EM and MM interactions have orbital components that lie outside rather than along the edges of the EM_3 tetrahedral cluster core. Hence, the requirements for good EM and MM bonding are competitive. Third, as bridging hydrogens lie outside the triangles making up the tetrahedron, they reinforce the bonding requirements of the bridged edge relative to the unbridged. It is the balance of these three factors that determines the hydrogen distribution that is observed. This balance depends on the identity of E, cluster charge, and the number of endo hydrogens. These various analyses show that rather dramatic changes in the main-group moiety can be accompanied by small overall energy change because of the great flexibility of the cluster system in accommodating a variety of bonding situations.

Experimental Section

Photoelectron Spectra. The He I, 21.1 eV, spectrum of $II(CH_3)$ was obtained by using an instrument that has been described elsewhere.[27] Calibration was carried out by using an internal reference of Xe/Ar. Resolution was 40 meV (fwhm) and constant with electron energy. Band positions were assigned by using Ar (15.76 eV) and sometimes water (12.62) for calibration. Spectra were gathered with a sample temperature of 42 °C. Sublimation was clean, and there was no evidence of CO gas, the usual decomposition product, in the spectra.

Calculations. The ab initio calculations were carried out by using the GAUSSIAN 80 programs.[28] Unless stated otherwise, all bond lengths, bond angles, and dihedral angles were optimized with no overall molecular symmetry constraints by using the minimal STO-3G basis set.[29] Geometry searches used analytical gradient routines based on the methods of Murtagh and Sargent.[30] Single-point calculations at the optimized geometries using more flexible basis sets[31] and iterative solution of the CI equations involving all single and double substitutions were used to refine the energies.

The nonparameterized Fenske–Hall technique[32] was used to examine the metal clusters, and the parameters and the basis functions used are the same as those reported in earlier work.[33] Extended Hückel parameters were the same as those used previously.[13] Geometries were based on crystallographic information from $H_3Fe_3(CO)_9CCH_3$[11] and $HFe_3(CO)_9(H_3BH)$.[7] Pertinent bond distances (Å) used are as follows: CH(t), 1.09; BH(t), 1.19; CH(μ), 1.19; BH(μ), 1.35; CFe, 2.00; BFe, 2.20; FeFe, 2.62; FeH(Fe), 1.56 ("tilt"), 1.64 ("flat"), FeH(C), 1.75; FeH(B), 1.60; FeC, 1.80; CO, 1.13. Structures were idealized to the highest symmetry possible.

Acknowledgment. The support of the National Science Foundation (CHE 8408251) is gratefully acknowledged as is the Computing Center of the University of Notre Dame for providing computational time. This research was also supported in part by the Office of Basic Energy Science of the Department of Energy (D.M.C.). This is Document No. NDRL-2899 from the Notre Dame Radiation Laboratory. Prof. H. Kaesz is thanked for providing coordinates from a cluster structure determination and Dr. C. Eigenbrot for aid in the analysis of the crystallographic data. The comments of Prof. J. F. Liebman on an earlier version of this manuscript are also appreciated.

Registry No. I(H), 76831-04-4; $I(CH_3)$, 69440-00-2; II(H), 91128-40-4; $II(CH_3)$, 101834-61-1; IIIa, 81940-45-6; IIIc, 110098-13-0; $[Fe(CO)_9BH]^{4-}$, 110098-11-8; $[Fe_3(CO)_9CH]^{3-}$, 110098-12-9; $[HFe_3(CO)_9(HCH)]^-$, 97920-76-8; $[Fe_3(CO)_9BH_4]^-$, 101810-38-2.

Supplementary Material Available: Tables showing trends in Mulliken charges and overlap populations for $Fe_3(CO)_9CH_4$, $[Fe_3(CO)_9CH_3]^-$, $Fe_3(CO)_9BH_5$, and $[Fe_3(CO)_9BH_4]^-$ from Fenske–Hall calculations and summarizing the $CH^-/Fe_3(CO)_9^{2-}$ and $BH^{2-}/Fe_3(CO)_9^{2-}$ fragment analyses (26 pages). Ordering information is given on any current masthead page.

(26) A theoretical analysis of CHM formation in mononuclear compounds shows that depopulation of a CH bonding orbital is the cause of CH bond weakening. Saillard, J.-Y.; Hoffmann, R. *J. Am. Chem. Soc.* **1984**, *106*, 2006. On the other hand, an examination of CH activation on metal surfaces via calculational methods suggests that population of a CH antibonding orbital is the most important initial effect of CH metal interaction. Baetzold, R. *J. Am. Chem. Soc.* **1983**, *105*, 4271. For other theoretical studies defining the nature of agostic interactions, see: Demolliens, A.; Jean, Y.; Eisenstein, O. *Organometallics* **1986**, *5*, 1457 and references therein.

(27) DeKock, R. L.; Wong, K.-S.; Fehlner, T. P. *Inorg. Chem.* **1982**, *21*, 3203.

(28) Binkley, J. S.; Whiteside, R. A.; Krishnan, R.; Seeger, R.; DeFrees, D. J.; Schlegel, H. B.; Topiol, S.; Dahn, L. R.; Pople, J. A. *QCPE* **1981**, *13*, 406. IBM version: van Kampen, P. N.; de Leeuw, F. A. A. M.; Smits, G. F.; Altona, C. Department of Chemistry, State University of Leiden, The Netherlands.

(29) Hehre, W. J.; Stewart, R. F.; Pople, J. A. *J. Chem. Phys.* **1969**, *51*, 2657.

(30) Murtaugh, B. A.; Sargent, R. W. H. *Comp. J.* **1980**, *13*, 185.

(31) 3-21G basis set: Binkley, J. S.; Pople, J. A.; Hehre, W. J. *J. Am. Chem. Soc.* **1979**, *102*, 939. 6-31G basis set: Hehre, W. J.; Ditchfield, R.; Pople, J. A. *J. Chem. Phys.* **1972**, *56*, 2257.

(32) Hall, M. B.; Fenske, R. F. *Inorg. Chem.* **1972**, *11*, 768. Hall, M. B. Ph.D. Thesis, University of Wisconsin, Madison, WI, 1971. Fenske, R. F. *Pure Appl. Chem.* **1971**, *27*, 61.

(33) Fehlner, T. P.; Housecroft, C. E. *Organometallics* **1984**, *3*, 764.